

Expanded Synthesis of 3D Covalent Organic Frameworks via Linker Exchange for Efficient Photocatalytic Aerobic Oxidation

WeiJie Zhang, Zhou Lu, Cailing Chen, Peter Vannatta, Chenxin Yang, Abdullah M. Al-Enizi, Ayman Nafady, and Shengqian Ma*

Despite recent progress in 3D covalent organic frameworks (3D-COFs), their design and synthesis still pose significant challenges, mainly due to a limited mechanistic understanding of their synthesis. Herein, a linker exchange approach has been utilized to synthesize a series of new 3D-COFs by first preparing an imine-linked 3D-COF followed by exchanging with selected linear diamine linkers. This approach can be widely applicable to different types of diamines, enabling rational-designed synthesis of 3D frameworks that are previously inaccessible via direct polymerization in a one-pot reaction. Mechanistic aspects associated with the improved 3D-COF synthesis via the linker exchange approach, are investigated by density functional theory calculations, in which the possibility of the departure of the leaving linker is a spontaneous process with a decrease in enthalpy. Catalytic and computational results revealed that incorporating benzoxazole moiety into the 3D-COF frameworks enables a significant increase in the capability of visible-light-driven catalysis. The overall findings of the present study will pave the way toward the development of 3D-COFs with tunable structures and functions for other promising and challenging applications.

1. Introduction

As a novel class of crystalline organic polymers, covalent organic frameworks (COFs) have attracted wide interest since first discovered by the Yaghi group in 2005.^[1] The first 3D-COF was presented in 2007 by the same group.^[2] However, the development of 3D-COFs has been relatively slow in comparison with 2D-COFs,^[3] mainly due to their limited synthetic methodology. Their topology determines that 3D-COFs have more complicated pore structures such as cages, interpenetrated channels, and numerous open sites. Owing to these structural properties, 3D-COFs show more advantages in gas storage,^[4] and separation,^[5] catalysis,^[6] energy storage,^[7] and encapsulation.^[8] However, as the driving force for 3D-COF construction relies only on the covalent bonds, it has proven to be a significant challenge for their design and synthesis, especially for the covalent linkages based on irreversible condensation reactions.^[9]

Recently, emerging techniques, including interfacial polymerization techniques at the air/water, liquid/liquid, liquid/solid, and solid/vapor interface,^[10] topology-templated synthesis,^[11] microwave and mechanical synthesis,^[12] multicomponent reaction and multistep synthesis strategies,^[13] linker-exchange strategy,^[14] chemical reconstruction,^[15] and two-step seeded growth approach^[16] have been employed to synthesize crystalline 2D-COFs. Until now, there are only a few examples of how new synthetic methodology contributes to the 3D-COFs. For instance, using ionic liquid (IL) as a green solvent has been reported to prepare a series of 3D ionic liquid-containing COFs (3D-IL-COFs).^[17] Reversible topological reaction based on light-induced [4 + 4] or [2 + 2] cycloaddition realizes the transformation between 2D-COFs and 3D-COFs.^[18] Z. Li et al. have reported the COF transformation from 3D-COFs to 3D-COFs for the first time by using heterogeneous linker exchange methodology under solvothermal conditions. This work provides a promising way for constructing new 3D-COFs which may be difficult in direct synthesis by one step.^[19] Compared to these methods, the linker exchange of COFs with targeted functions is a facile synthetic approach (Table S1, Supporting Information). Therefore, it is

W. Zhang, Z. Lu, P. Vannatta, S. Ma
Department of Chemistry
University of North Texas
Denton, TX 76203, USA
E-mail: Shengqian.Ma@unt.edu

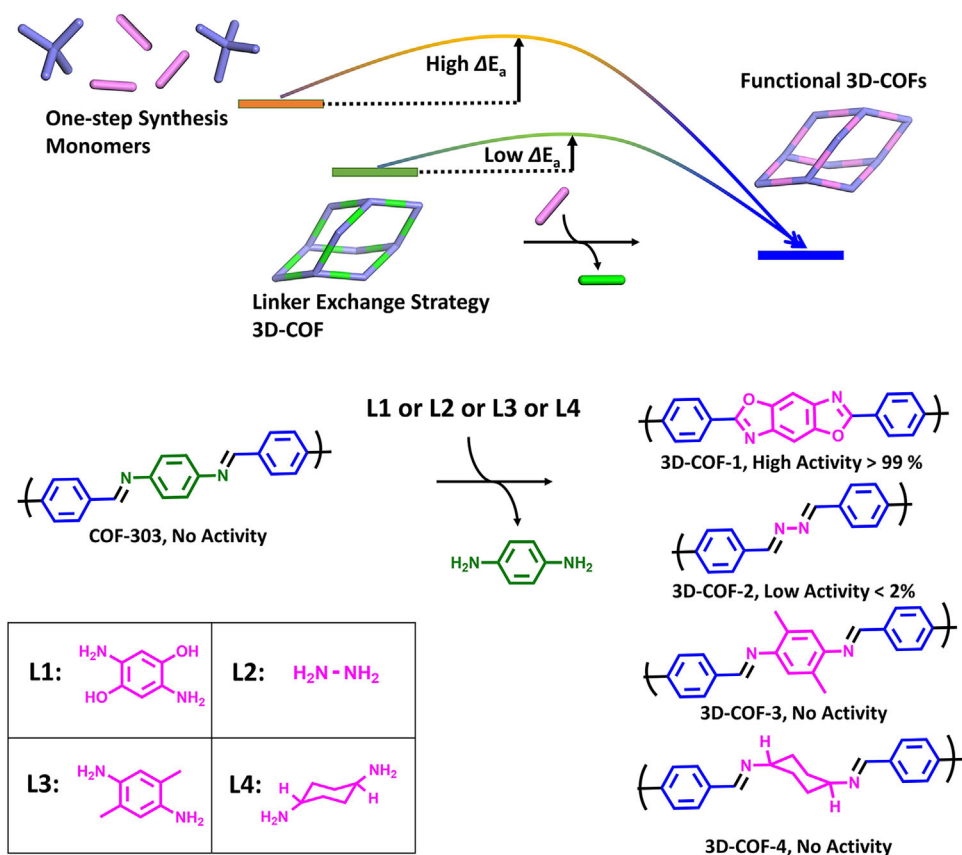
C. Chen
Advanced Membranes and Porous Materials Center
Physical Sciences and Engineering Division
King Abdullah University of Science and Technology
Thuwal 23955-6900, Saudi Arabia

C. Yang
Department of Chemistry
University of Virginia
Charlottesville, VA 22903, USA

A. M. Al-Enizi, A. Nafady
Department of Chemistry
College of Science
King Saud University
Riyadh 11451, Saudi Arabia

The ORCID identification number(s) for the author(s) of this article can be found under <https://doi.org/10.1002/sml.202502316>

DOI: 10.1002/sml.202502316



Scheme 1. Differences in the synthesis of 3D-COFs by one-step synthesis and linker exchange strategy and their catalytic performance in the transformation of arylboronic acids to phenols.

desirable to gain a mechanistic understanding and to achieve a universal approach for regulating the synthesis of functional 3D-COFs.

Recently, a concise introduction of reticular chemistry to dynamic covalent chemistry has been successfully implemented for the synthesis of new classes of porous materials.^[20] As the reaction re-equilibrates toward the global minimum to form the most thermodynamically stable crystalline products, higher-ordered crystalline products can be easily obtained by using weaker covalent bonds. This also validates the possibility of exchanging COFs that are constructed by weaker covalent bonds with other linkers that form stronger covalent bonds. Most 3D-COFs are synthesized through one-pot solvothermal methods, thereby posing a significant challenge in exerting deliberate control over 3D-COF skeletons. Thermodynamic control dominates in the 3D-COF formation from the traditional one-pot solvothermal methods by overpassing a large energy barrier. As shown in Scheme S1 (Supporting Information), the rapid generation of an amorphous polymer under kinetic control results in elevated energy barriers ($\Delta E_{a1} \gg \Delta E_{a2}$), compared to using 3D-COF as the intermediate materials. However, it is feasible to transform the thermodynamically favorable processes into kinetically favorable processes by lowering the enthalpy change from predetermined arrangements of starting materials ($\Delta H_1 > \Delta H_2$). Furthermore, such a strategy will not only take full advantage of the template effect stemming

from the 3D frameworks but also inherit the practical functions from targeted linkers.

In this contribution, our central hypothesis is that the reaction can start via raw materials from as-synthesized COFs rather than the monomers (Scheme 1). In particular, we targeted the COF containing a 3D multifold interpenetrating diamond-like structure.^[8a,17,21] COF-303 was synthesized by the self-condensation of a tetrahedral aldehyde (tetrakis(4-formylphenyl)methane, TFM) with a linear diamine (phenylenediamine, PDA). To demonstrate the proposed approach in practice, four types of diamine linkers including 2,5-diaminohydroquinone dihydrochloride (L1), hydrazine (L2), 2,5-dimethyl-1,4-benzenediamine (L3) and *trans*-1,4-cyclohexanediamine (L4) have been selected to produce new 3D-COFs via a diamine linker exchange strategy. Four different 3D-COFs (identified herein as 3D-COF-1, 3D-COF-2, 3D-COF-3, and 3D-COF-4) with distinct ordered framework structures were obtained, which offered promising candidates for photocatalysis. To the best of our knowledge, our work represents the first case of benzoxazole-linked and cyclohexanediamine-based 3D-COFs. Mechanistic investigation of linker-exchange reactions revealed that the process follows a kinetically favorable strong-weak base substitution mechanism. The prerequisite or the driving force is that the diamine linker with comparably strong base properties (high pK_a value) replaces the PDA linker (low pK_a value) on

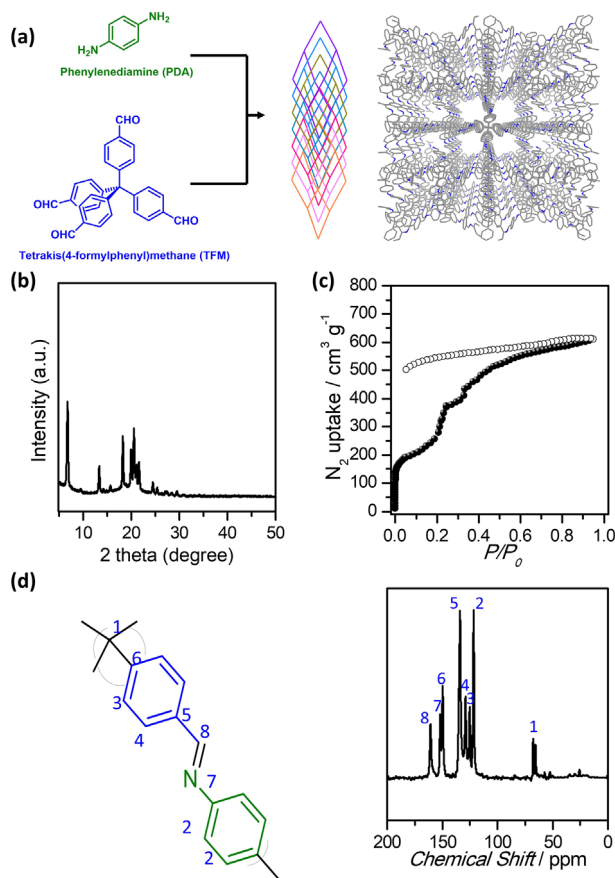


Figure 1. a) Reversible dynamic covalent bond formation (imine condensation) between TFM and PDA to produce *dia-c7* COF-303. It crystallizes in the space group $I4_1/a$ with *dia* topology and a sevenfold interpenetrated framework. b) PXRD patterns of solvated *dia-c7* COF-303. c) Nitrogen adsorption (filled symbol) and desorption (open symbol) isotherm for *dia-c7* COF-303 measured at 77 K. d) Solid-state ^{13}C CP-MAS spectrum of synthesized *dia-c7* COF-303 material.

template COF-303. Moreover, 3D-COF-1 displayed outstanding activity in the visible-light-driven oxidative hydroxylation of arylboronic acids due to a density of benzoxazole moiety that is well arranged into the nano-space.

2. Results and Discussion

2.1. Syntheses and Characterizations

In a typical experiment, a vial was charged with tetrakis(4-formylphenyl)methane (TFM), 1,4-phenylenediamine (PDA), and a mixture of 1,4-dioxane and mesitylene; then aqueous acetic acid was added to the solution followed by heating to 120 °C to yield crystalline solids.^[22] The crystallinity of solvated COF-303 was confirmed by powder X-ray diffraction (PXRD) analysis in which all peaks have been indexed on a tetragonal unit cell with parameters ($a = b = 26.47 \text{ \AA}$, $c = 7.45 \text{ \AA}$) (Figure 1b; Figure S3, Supporting Information). Note that these parameters are distinct from those of *dia-c7* ($a = b = 20.41 \text{ \AA}$ and $c = 8.82 \text{ \AA}$, Figure S4, Supporting Information). In particular, no other diffraction peaks from the starting materials (PDA and TFM) were observed

in COF-303 (Figure S5, Supporting Information). All the peaks in the PXRD pattern of activated COF-303 could also be indexed in Figure S6 (Supporting Information). Additionally, the permanent porosity of COF-303 was successfully established by measuring N_2 adsorption at 77 K (Figure 1c). The observed hysteresis suggested that as-synthesized COF-303 changes its pore structure during the adsorption-desorption process, which is in accordance with the results from the PXRD analysis (Figure S6, Supporting Information). The Brunauer–Emmett–Teller (BET) surface areas were determined as $920 \text{ m}^2 \text{ g}^{-1}$ (within the range of $0.02 < P/P_0 < 0.2$). The *dia-c7* COF-303 was confirmed with a crystal dimension of $\approx 100 \text{ nm}$ (Figures S7 and S8, Supporting Information) which was thermally stable up to 300 °C (Figure S9, Supporting Information).

The solid-state ^{13}C cross-polarization magic-angle-spinning NMR (^{13}C CP-MAS) spectrum indicated the presence of carbon from the C=N bond at 160 ppm (Figure 1d). ^{13}C NMR of COF-303 showed two different sp^3 carbons. This observation aligns with the findings from similar studies, such as the Yaghi group's work on COF-300, which also exhibited two different sp^3 carbons.^[8a] This has also been observed in the 2D-COF framework.^[23] The presence of these distinct sp^3 carbon environments may suggest a highly ordered and well-defined structure in COF-303, corroborating the high quality of the material. Another reason may be the constitutional isomerism of imine linkages, which has rarely been considered so far as an essential aspect.^[24] For example, one in which the monomer is linked to the imine carbon (A-C = N-B) and the other where it is linked to the imine nitrogen (A-N = C-B). The NMRs of the linker-exchanged COF are much broader, implying an increased disorder that is in line with the drop of surface area.

With this material in hand, the exchange process was undertaken using 2,5-diaminohydroquinone dihydrochloride (L1) as the functionalized linker (Figure 2a). Linker exchange was conducted by exposing the COF-303 to one, two, or four equivalents of L1 with respect to PDA at 85 °C for 2 days. The isolated solid was then washed with hot THF, DCM, and ethanol before overnight activation under a dynamic vacuum at 120 °C. Following linker exchange on COF-303, deep brown 3D-COF-1 powder was obtained with crystallinity confirmed (Figure 2b; Figure S10, Supporting Information) and the same topology as COF-303 (Figure S11, Supporting Information) determined by PXRD. The porosity of the 3D-COF-1 and benzoxazole-functionalized 3D-COF-1 was investigated via nitrogen sorption experiments (Figure 2c; Figures S12–S14, Supporting Information). The benzoxazole-functionalized 3D-COF-1 exhibited a lower BET surface area ($645 \text{ m}^2 \text{ g}^{-1}$) than that of the pristine COF-303 ($920 \text{ m}^2 \text{ g}^{-1}$). Further, the expected signal shifts appeared in the FT-IR spectrum at $1621 \text{ m}^2 \text{ g}^{-1}$, $1604 \text{ m}^2 \text{ g}^{-1}$, and $1569 \text{ m}^2 \text{ g}^{-1}$ (Figure 2d; Figure S12, Supporting Information). Notably, 3D-COF-1 is the first example of an oxazole 3D-COF with crystallinity (Figure S15, Supporting Information). Solid-state ^{13}C CP-MAS characterization of the activated materials supports the conversion to the benzoxazole linkage (Figure S16, Supporting Information). In addition, 3D-COF-1 showed no significant difference in morphology between COF-303 and 3D-COF-1 as indicated by scanning electron microscopy (SEM) images (Figure S17, Supporting Information). Its thermal stability up to 300 °C was evidenced by TG analysis (Figure S18, Supporting Information).

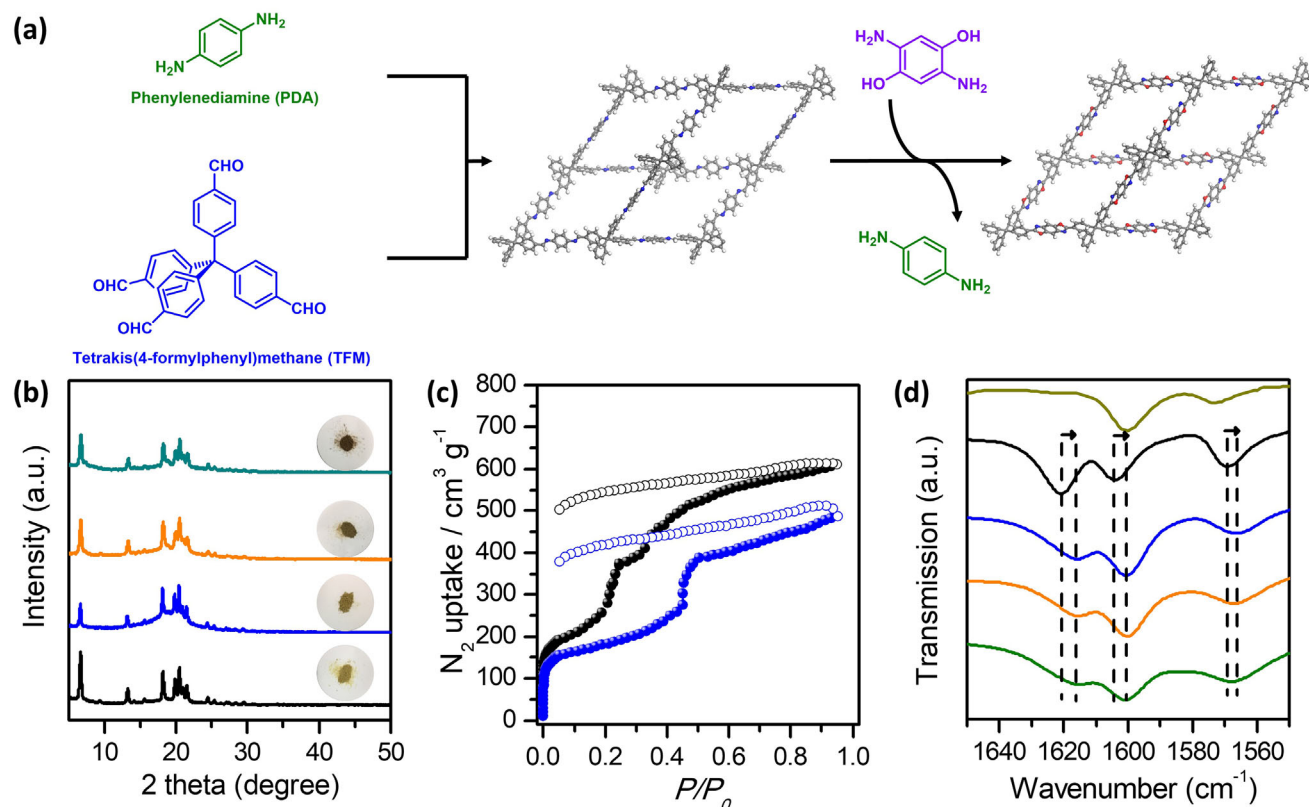


Figure 2. a) Synthesis scheme of **3D-COF-1** by post-synthetic linker exchange, the reversible imine condensation between TFM and PDA produces COF-303, and subsequent exchange reaction involving the substitution of one to four equivalents of 2,5-diaminohydroquinone dihydrochloride (**L1**). b) Transformation from solvated COF-303 to solvated **3D-COF-1** in different equivalents of **L1** indicated by PXRD patterns and photographs, showing retention of crystallinity (COF-303, black; 1 eq. of **L1**, blue; 2 eq., orange; 4 eq., green). c) Nitrogen sorption isotherms, performed at 77 K, showing permanent porosity of **3D-COF-1** (blue) compared to that of COF-303 (black). Solid and open circles indicate adsorption and desorption, respectively. d) FT-IR spectra of the prepared 3D-COFs, with characteristic imine stretch indicated (TFM, olive; COF-303, black; 1 eq. of **L1**, blue; 2 eq., orange; 4 eq., green).

To confirm the versatility of our general approach, post-synthetic exchange was successful in achieving three additional new 3D-COFs for which the corresponding imine-linked frameworks have not yet been reported. In general, the synthesized **3D-COF-2**, **3D-COF-3**, and **3D-COF-4** exhibited excellent crystallinities (Figure 3a–c) with surface areas of 251, 745, and 616 m² g⁻¹, respectively (Figure 3d–f). Furthermore, the characterizations of **3D-COF-2**, **3D-COF-3** and **3D-COF-4** by solid-state ¹³C CP-MAS, FT-IR spectra, SEM images, and TG, are consistent with conversion to the corresponding linkages (Figures S19–S22, Supporting Information for **3D-COF-2**, Figures S23–S26, Supporting Information for **3D-COF-3**, Figures S27–S30, Supporting Information for **3D-COF-4**). We observed that attempts to synthesize **3D-COFs** via direct condensation could not result in the formation of any crystalline powder (Figures S31 and S32, Supporting Information), indicating that the desired framework structures could not be achieved under the same conditions.

However, it should be noted that when **L2** was applied, the azine-linked **3D-COF-2** crystallized in a diamond network and likely with different interpenetration degrees (Figure S33, Supporting Information). Its crystallinity was confirmed by PXRD in which all peaks were indexed on a space group P₄₂/n (Figure S34, Supporting Information). In Figure S34 (Supporting Infor-

mation), we compared the experimental PXRD pattern of **3D-COF-2** and the simulated PXRD patterns of fourfold to sevenfold interpenetrated structures. The PXRD pattern of **3D-COF-2** matches well with that of the 6-fold interpenetrated. These parameters are similar to the recently reported ones of *dia-c6* (trigonal unit cells with a = b = 13.20 Å, c = 7.44 Å)^[25] and distinct from previously reported ones of *dia-c2* (tetragonal unit cells with a = b = 15.14 Å, c = 19.97 Å).^[26] Since no changes were observed in the topology of other 3D frameworks, this structural reconstruction could be mainly attributed to the significant difference in the length of diamines. Interestingly, there was no significant change in the PXRD patterns of solvated and activated **3D-COF-2** (Figure S35, Supporting Information). Like **3D-COF-1**, a decrease of crystallinity was expected for the **3D-COF-3** and **3D-COF-4**, especially for excess of linker exchange (Figures S36 and S37 (Supporting Information) for **3D-COF-3** and Figures S38 and S39 (Supporting Information) for **3D-COF-4**). Upon the exchange of linker **L3** with COF-303, the surface areas decreased from an initial 920 to 529 m² g⁻¹, respectively (Figures S40 and S41, Supporting Information). The integration of the linker **L4** in COF-303 also resulted in a surface area decrease to 364 m² g⁻¹ (Figures S42 and S43, Supporting Information). Additionally, we anticipated that the flexibility of the **L4** linker would

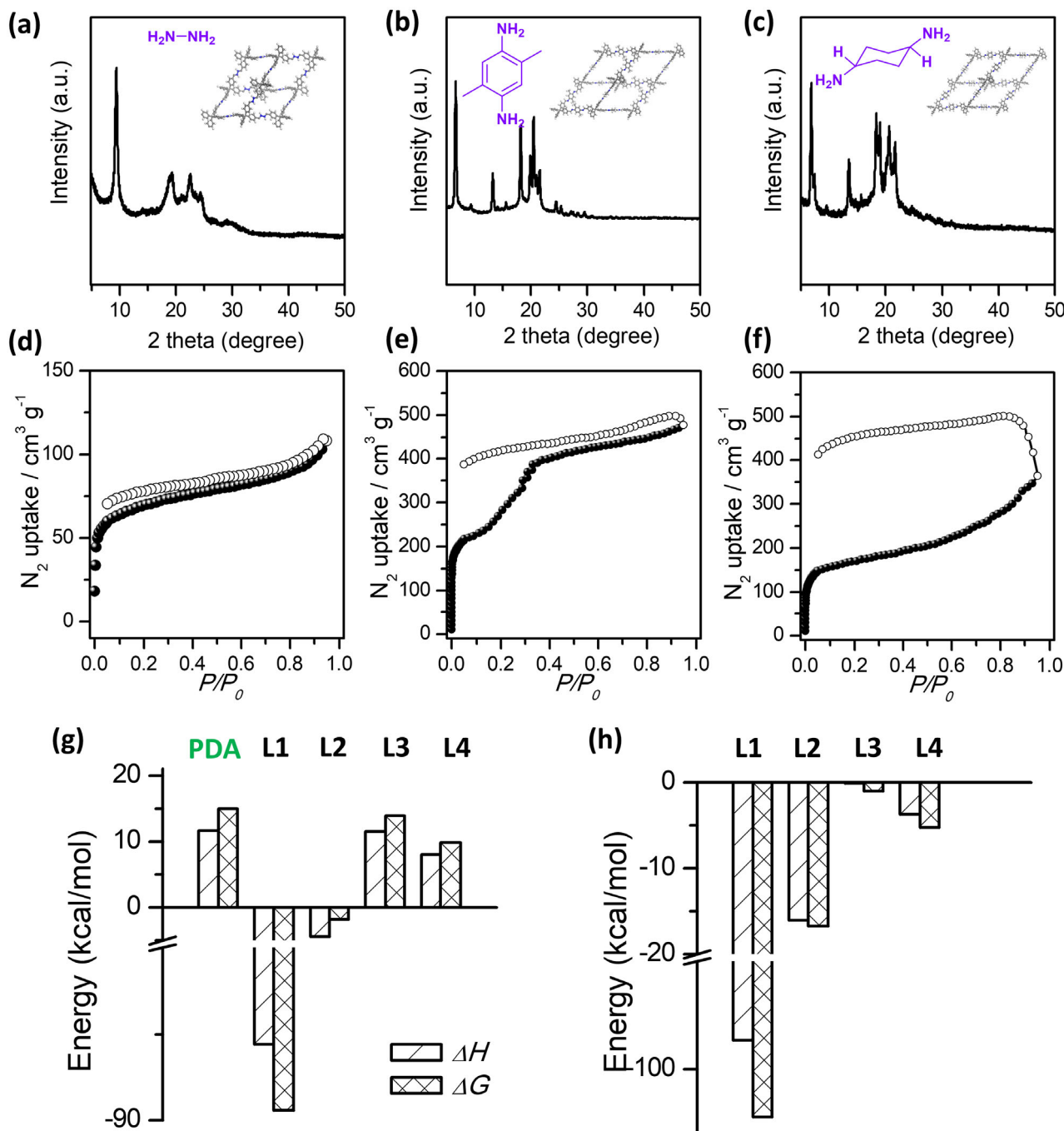


Figure 3. a–c) PXRD patterns of solvated **3D-COF-2**, **3D-COF-3**, and **3D-COF-4** by post-synthetic linker exchange, showing retention of crystallinity. d–f) Nitrogen sorption isotherms, performed at 77 K, show the permanent porosity of **3D-COF-2**, **3D-COF-3**, and **3D-COF-4**. Solid and open circles indicate adsorption and desorption, respectively. g) Density functional theory (DFT) calculated deriving enthalpies (ΔH) and Gibbs free energies (ΔG) of homogeneous condensation to form two imine bonds between diamine linkers (PDA, L1, L2, L3 and L4) and benzaldehyde. h) DFT-derived enthalpies (ΔH) and Gibbs free energies (ΔG) of the linker-exchange reaction with *N,N'*-dibenzylidene-1,4-phenylenediamine diamines (L1, L2, L3 and L4).

somewhat impede the structural linker distortion in the framework, leading to the larger hysteresis observed during the adsorption-desorption process (Figure 3f).

To further examine the completeness of the conversion reaction, the COFs were hydrolyzed by concentrated HCl. As only for COF-303 and **3D-COF-3**, the solid suspension in concentrated

HCl disappeared to form a clear and transparent solution, indicating a complete hydrolysis. However, amine hydrochloride has low solubility in CDCl_3 . Therefore, the peaks corresponding to protons of Tetrakis(4-formyl phenyl)methane (TFM) were identified after the acidic treatment (Figure S44, Supporting Information). In contrast, **3D-COF-1** remained a non-hydrolyzable solid

after the same treatment, suggesting its much higher chemical stability. Moreover, no signals corresponding to TFM were observed in the ^1H NMR spectrum of **3D-COF-1**, indicating a complete imine-to-oxazole conversion (Figure S44a, Supporting Information). A similar result was also observed for **3D-COF-2** and **3D-COF-4** with weak signals of TFM in the ^1H NMR spectrum. The increased chemical stability of the resultant crystallites further corroborates the successful structural conversion from the COF-303 to the 3D-COFs.

To address the solubility issue of amine hydrochloride, $\text{DMSO-}d_6$ was used instead of CDCl_3 . The molar ratio of TFM to 1,4-phenylenediamine (PDA) was calculated to be 1:2 based on integrals of the peaks, in full agreement with the COF-303 structure (Figure S45, Supporting Information). Consequently, the linker exchange efficiency can be determined by analyzing the ratio of outgoing PDA to total PDA through ^1H NMR. For **3D-COF-3**, the decrease in abundance of protons at 7.28 ppm in ^1H NMR indicated the PDA moieties are replaced by the incoming **L3** linkers. The ratio of outgoing PDA to total PDA was calculated $\approx 0.3:1$ at 2.5 h and 1:1 at 48 h, indicating 30% PDA and 100% PDA replaced by **L3**, respectively (Figure S46, Supporting Information). Furthermore, solid UV-vis spectra of **3D-COF-2** and **3D-COF-4** samples showed that there is almost no absorbance in the 500–800 nm wavelength range upon linker exchange, confirming that the PDA has been completely substituted (Figure S47, Supporting Information).

The contribution of enthalpies toward the linker exchange approach was elucidated by density functional theory (DFT) calculations. The possibility of the departure of the outgoing linker can be governed by the ΔH and ΔG values. For the homogeneous condensation (or the dynamic covalent bond formation) between diamines (PDA, **L1**, **L2**, **L3**, and **L4**) and benzaldehyde in Scheme S2 (Supporting Information), no obvious principles could be accounted for the one-step imine formation (Figure 3g). A similar trend was observed for the other one-step imine formations starting from different numbers or types of amine linkers (Figures S48–S50, Supporting Information). That is, the comparatively negative ΔH and ΔG values hint that once the linkage is formed, it is difficult to reverse the condensation or break the covalent bonds. The formation of benzoxazole-linked ultra-stable frameworks process requires multiple steps and base as a catalyst, including imine formation, cyclization reaction, both oxidation and dehydrogenation reaction, harsh conditions (185 °C, 5 days), and benzimidazole as a base catalyst, which has been verified recently.^[13a] However, in this case, the linker exchange method only needs mild conditions, O_2 to produce H_2O as a by-product but also avoids the utilization of a base catalyst.^[14b] The oxazole linkage was thermally stable with limited reversibility, which accounts for the particular synthesis challenge. However, for the PDA linker, the positive ΔH and ΔG values indicated that the corresponding condensations into dynamic imine bonds are highly reversible. This accounts for the amorphous polymer formation via azole linkages under kinetic control and COF-303 formation via imine linkages under thermodynamic control. In order to explain the substitution, we proposed a homogeneous linker-exchange reaction, similar to the imine bond formation via the condensation of aniline with benzaldehyde (Scheme S2, Supporting Information). In the same manner, the energy profiles of linker-exchange reactions involving Salen-type linkers

were explored (Scheme S3, Supporting Information). For example, the negative ΔH and ΔG values indicated that the Salen-type and incoming **L1** are limited reversible and kinetically favorable, thereby allowing for the spontaneous formation of more stable oxazole compounds with the PDA leaving (Figure 3h). In this regard, a similar protocol can be utilized to examine whether the synthesis of COF using the other three linkers can occur in a linker-exchange manner. Spontaneous linker exchange from the incoming linker to the outgoing linker is accompanied by the loss of enthalpy. Such a process also takes full advantage of the template effect stemming from the 3D frameworks, leading to improved synthesis of 3D-COF with functions from incoming linkers.

Current theoretical and experimental findings revealed that both the ΔH and ΔG values play a crucial role in governing the linker substitution reactions. High-performance liquid chromatography (HPLC) was employed to analyze the released PDA. The solutions after filtration were taken from the vials and analyzed by HPLC equipped with a UV-vis detector. Obviously, **L1** has a higher linker exchange rate compared to other linkers (Figure S51d, Supporting Information). The evident relationship between the linker exchange rate of COF and its $\text{p}K_a$ value was probed to correlate the DFT calculations. We further envisioned that the basicity of the diamine linker in the 3D-COF can be used for estimating the possibility of an exchange reaction with respect to a specific approaching linker. The $\text{p}K_a$ values for the diamine linkers follow the order **L1** (10.24 ± 0.10) > **L4** (10.18 ± 0.10) > **L2** (8.18 ± 0.10) > **L3** (6.14 ± 0.10) \approx PDA (6.17 ± 0.10). In other words, the diamine Brønsted basicity also follows this order, indicating a proposed strong-weak base mechanism of linker exchange. That is, the more basic diamines can more easily drive linker substitution reactions than less basic ones. However, the $\text{p}K_a$ value of PDA is quite close to that of **L3**. Without experimental evidence, the substitution reaction becomes difficult to predict reliably. Therefore, it is worth calculating ΔH and ΔG values based on the proposed homogeneous linker exchange reaction to obtain a more reliable energy platform for linker exchange in future studies.

2.2. Catalytic Performance and Mechanism Study

Phenols serve as versatile building blocks and intermediates in the current chemical and pharmaceutical industries.^[27] Meta-substituted phenols can be obtained via a one-pot C–H borylation/oxidation sequence that would be challenging by other methods. For oxidation, many straightforward methods have been developed for the conversion of arylboronic acids into phenols, with practical and economic challenges.^[27,28] Thus, there still exists an opportunity to develop catalytic systems to efficiently convert arylboronic acid into phenols. In this respect, photocatalytic aerobic oxidation has been widely considered a new and environmentally benign approach. In this area, the Xiao and Scaiano research groups have elucidated that superoxide radical anion (O_2^-), readily obtained via photo-excitation of molecular oxygen (O_2) in the presence of a sacrificial reductant, is competent for the conversion of arylboronic acids to phenols.^[28c,d] Recently, the Wang group reported that benzoxazole-linked 2D-COFs exhibit excellent activity, high stability, broad universality for substrates, and expected recyclability as a metal-free

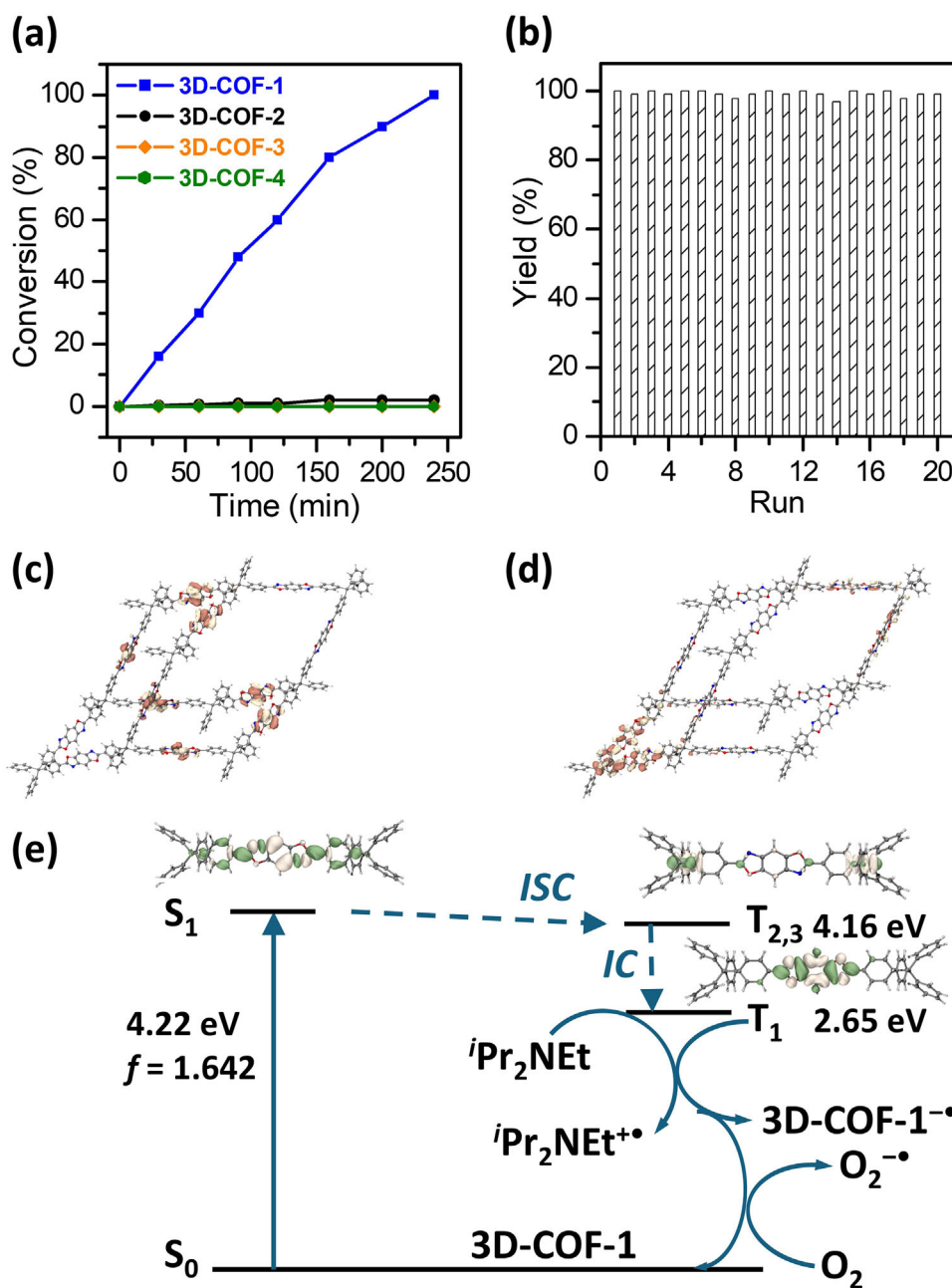


Figure 4. a) Photocatalytic activity test of 3D-COF-1, 3D-COF-2, 3D-COF-3, and 3D-COF-4 in the oxidative hydroxylation of phenylboronic acid to phenol. b) Assessment of the reusability of 3D-COF-1 in photo-catalyzing the oxidative hydroxylation of phenylboronic acid. The reusability studies have been undertaken under identical conditions. c) HOMO and d) LUMO contours (isovalue = 0.015 a.u.) of 3D-COF-1 fragment. e) Proposed Jablonski diagram and photocatalytic mechanism of 3D-COF-1 in activation of O_2 . Inset figures are electron density difference (EDD) maps of corresponding excited states with isovalues of 0.0005 a.u. ISC = inter-system crossing; IC = internal conversion.

heterogeneous photocatalyst in the same catalytic system.^[13a] Therefore, visible-light-promoted aerobic oxidation of arylboronic acids was chosen to examine the photocatalytic activity of 3D-COF-1, 3D-COF-2, 3D-COF-3, and 3D-COF-4.

The transformation of phenylboronic acid to phenol was first selected as the model evaluation reaction. Factors that could affect this reaction were carefully assessed by control experiments, and the obtained results are listed in Table S2 (Supporting In-

formation). A yield of $\approx 99\%$ was accomplished by adopting 3D-COF-1 as the photocatalyst and iPr_2NEt as the sacrificial reagent in the air (entry 1). Moreover, in the absence of either oxygen source (entry 6), light (entry 7), or photocatalyst (entry 8), the reaction yield was significantly diminished. For comparison with 3D-COF-1, all of 3D-COF-2, 3D-COF-3, 3D-COF-4 and COF-303 were also tested (Figure 4a). 3D-COF-2 was less efficient (2% yield) under the same reaction conditions, whereas the 3D-COF-3,

3D-COF-4, and COF-303 showed no activity. Taken together, the combined data indicated that the remarkable photocatalytic activity arises from the benzoxazole-linked π -conjugated crystalline framework. Furthermore, the superiority of crystalline 3D-COF-1 as the photocatalyst was demonstrated by a comparison between our work and previously reported results (homogeneous catalysis and heterogeneous catalysis summarized in Table S3, Supporting Information), and recycling experiments (Figure 4b). 3D-COF-1 can be easily recycled from the reaction mixture and serve as a recyclable photocatalyst for the subsequent runs. Without any special treatment or pre-activation process, crystalline 3D-COF-1 showed high and unchanged activity even after 20 runs in the visible-light-driven transformation of phenylboronic acid (Figure 4b).

The substrate scope of arylboronic acids was investigated to illustrate the generality of 3D-COF-1 as a catalyst. As shown in Figure S53 (Supporting Information), in the presence of 3D-COF-1, a series of arylboronic acids with electron-withdrawing substituents have been efficiently transferred to the desired products in highly exceptional yields (> 99%). Other substrates with electron-donating substituents also experienced satisfactory conversion. Meanwhile, polycyclic substrates showed a size-dependence effect toward the reaction yields, dropping with increasing substrate size. For large-sized 1-pyrenylboronic acid, it cannot be smoothly accommodated within the pores of 3D-COF-1, leading to a lower yield (28%). This size selectivity does not exist in homogeneous systems, which highlights a unique feature of 3D-COF-1 as the photocatalyst. To gain insight into the photocatalytic role of 3D-COF-1, spin-trapping experiments were carried out and the trapped adduct was tested by electron spin resonance (ESR) spectroscopy. When 5,5-dimethyl-1-pyrroline N-oxide (DMPO) was added to the air-saturated methanol solution which contains the 3D-COF-1, the adduct of superoxide radical anion ($O_2^{\cdot-}$) trapped by DMPO was successfully detected after visible-light irradiation (Figure S54, Supporting Information). Compared to 3D-COF-1, the other 3D-COF catalysts produced a small amount of $O_2^{\cdot-}$, leading to relatively weak ESR signals.

Computational studies were conducted to gain insights into the photocatalytic behavior of 3D-COFs (Figure 4c,d; Figures S55–S59, Supporting Information). As shown in Figure 4c,d, the highest occupied (HOMO) and lowest unoccupied molecular orbitals (LUMO) of 3D-COF-1 are mainly localized in the benzoxazole-linked π -conjugated parts. Time-dependent density functional theory (TD-DFT) calculations further revealed the origins of excited states with the proposed Jablonski diagram and photocatalytic mechanism depicted in Figure 4e and Figures S60–S64 (Supporting Information). Compared with other 3D-COFs, the lowest singlet state (S_1) of 3D-COF-1 was excited by visible light with significant oscillator strength (f) of 1.642, followed by the inter-system crossing (ISC) to $T_{2,3}$ state and internal conversion (IC) to the lowest triplet state (T_1), whose origin was also localized excitation of benzoxazole-linker (Figure 4e). The triplet 3D-COF-1 was reduced by the sacrificial reagent iPr_2NET , followed by the electron transfer to the dioxygen to give the active species $O_2^{\cdot-}$ and promote photocatalytic aerobic oxidation. This also accounts for the observed radicals with strong ESR signal intensities determined from 3D-COF-1. Therefore, 3D-COF-1 as a strong visible-light-absorbing sensitizer can dramatically boost photocatalytic activity through efficient electron transfer.

3. Conclusion

In this work, the COF-303 skeleton has been selected as the raw material rather than organic monomers, which was found to be compatible with post-synthetic functionalization with its porosity and crystallinity retained. The high porosity and crystallinity of post-synthesized 3D-COF materials attest to the value of the linker-exchange method. We successfully synthesized a series of 3D-COFs, including benzoxazole-linked, azine-linked and imine-linked 3D-COFs. Moreover, the channel walls were engineered with photocatalytic species in a simple yet controlled manner. The benzoxazole-linked π -conjugated crystalline 3D framework displayed excellent photocatalytic activity and recyclability.

Although recent synthetic developments offer an efficient approach to 2D-COF synthesis, these general predictive approaches are difficult to apply for 3D-COF preparation. In order to facilitate the linker-exchange approach, we developed a platform to elucidate the underlying principles, which remain elusive for 3D-COFs. Our findings address some of the associated hurdles in 3D-COF synthesis. This work indicated that 3D-COF preparation can be easily controlled through the judicious design of a step-wise synthetic pathway, enabling the synthesis of 3D-COFs previously synthetically inaccessible. Such a linker-exchange strategy is also an established and crucial step in many methods of MOF and 2D-COF synthesis.^[14c,19,29] Additionally, we have used DFT to calculate energy landscapes for the linker exchange process. Our results show that the exchange of monomers from the incoming to the outgoing monomer moieties was found to occur spontaneously and is exergonic. To correlate the DFT calculations, the relationship between the ligand exchange rate of COF and the pK_a value of exchanging linkers was probed to demonstrate a strong-weak base substitution mechanism as a more general principle of the linker exchange process. In addition to the enhancement of our fundamental understanding of structure-property relationships, we anticipate these results will be helpful in the production of novel 3D-COFs with readily tunable functionalities and high degrees of long-range crystalline order.

In conclusion, we have successfully demonstrated that the linker exchange strategy can promote the synthesis of novel 3D-COFs with predictable structures. The present study gives insight into the fundamentals of COF synthesis and provides new clues for the rational *de novo* synthesis of 3D-COFs. The combined experimental/computational studies revealed the possibility of kinetically controlling thermodynamically favorable processes through the utilization of predetermined arrangements of starting materials. Based on these results, it can be concluded that the more basic diamines readily drive the spontaneous departure of the leaving monomer with the release of enthalpy. Through this method, we have successfully synthesized four novel functionalized 3D-COFs; one of which displays an outstanding activity for the transformation of arylboronic acids to phenols due to a high density of photocatalytic species well-arranged in the nano-space. This contribution will be valuable for promoting the integration of crystallinity, stability, porosity, and a variety of functionalizations for broad application and is expected to greatly broaden the scope and advance the research progress of designed porous materials.

Supporting Information

Supporting Information is available from the Wiley Online Library or from the author.

Acknowledgements

W.Z. and Z.L. contributed equally to this work. The authors acknowledge the Robert A. Welch Foundation (B-0027) for financial support of this work. Partial support from the Researchers Supporting Program (RSP2025R55) at King Saud University, Riyadh, Saudi Arabia (AMA) is also acknowledged.

Conflict of Interest

The authors declare no conflict of interest.

Data Availability Statement

The data that support the findings of this study are available from the corresponding author upon reasonable request.

Keywords

covalent organic frameworks, expanded synthesis, linker exchange, photocatalysis

Received: March 8, 2025
Revised: March 10, 2025
Published online: March 20, 2025

- [1] A. P. Cote, A. I. Benin, N. W. Ockwig, M. O'Keeffe, A. J. Matzger, O. M. Yaghi, *Science* **2005**, *310*, 1166.
- [2] H. M. El-Kaderi, J. R. Hunt, J. L. Mendoza-Cortes, A. P. Cote, R. E. Taylor, M. O'Keeffe, O. M. Yaghi, *Science* **2007**, *316*, 268.
- [3] a) Z. Zhou, L. Zhang, Y. Yang, I. J. Vitorica-Yrezabal, H. Wang, F. Tan, L. Gong, Y. Li, P. Chen, X. Dong, Z. Liang, J. Yang, C. Wang, Y. Hong, Y. Qiu, A. Golzhauser, X. Chen, H. Qi, S. Yang, W. Liu, J. Sun, Z. Zheng, *Nat. Chem.* **2023**, *15*, 841; b) C. Kang, Z. Zhang, S. Kusaka, K. Negita, A. K. Usadi, D. C. Calabro, L. S. Baugh, Y. Wang, X. Zou, Z. Huang, R. Matsuda, D. Zhao, *Nat. Mater.* **2023**, *22*, 636; c) X. Guan, F. Chen, S. Qiu, Q. Fang, *Angew. Chem., Int. Ed.* **2023**, *62*, e202213203; d) X. Wang, Y. Wada, T. Shimada, A. Kosaka, K. Adachi, D. Hashizume, K. Yazawa, H. Uekusa, Y. Shoji, T. Fukushima, M. Kawano, Y. Murakami, *J. Am. Chem. Soc.* **2024**, *146*, 1832; e) C. Gropp, T. Ma, N. Hanikel, O. M. Yaghi, *Science* **2020**, *370*, eabd6406; f) J. Ding, X. Guan, J. Lv, X. Chen, Y. Zhang, H. Li, D. Zhang, S. Qiu, H. L. Jiang, Q. Fang, *J. Am. Chem. Soc.* **2023**, *145*, 3248; g) Y. Yin, Y. Zhang, X. Zhou, B. Gui, G. Cai, J. Sun, C. Wang, *J. Am. Chem. Soc.* **2023**, *145*, 22329; h) D. Zhu, Y. Zhu, Y. Chen, Q. Yan, H. Wu, C. Y. Liu, X. Wang, L. B. Alemany, G. Gao, T. P. Senftle, Y. Peng, X. Wu, R. Verduzco, *Nat. Commun.* **2023**, *14*, 2865; i) X. Han, S. E. Neumann, B. L. Nannenga, K. Wang, K. K. Li, S. Mirzaei, X. Yao, C. Zhu, M. Y. Gao, Y. B. Zhang, Y. Cui, O. M. Yaghi, *J. Am. Chem. Soc.* **2023**, *145*, 22885; j) J. Han, J. Feng, J. Kang, J. M. Chen, X. Y. Du, S. Y. Ding, L. Liang, W. Wang, *Science* **2024**, *383*, 1014; k) H. S. Xu, Y. Luo, P. Z. See, X. Li, Z. Chen, Y. Zhou, X. Zhao, K. Leng, I. H. Park, R. Li, C. Liu, F. Chen, S. Xi, J. Sun, K. P. Loh, *Angew. Chem., Int. Ed.* **2020**, *59*, 11527; l) B. Gui, G. Lin, H. Ding, C. Gao, A. Mal, C. Wang, *Acc. Chem. Res.* **2020**, *53*, 2225.
- [4] Y. Yin, Y. Zhang, X. Zhou, B. Gui, W. Wang, W. Jiang, Y. B. Zhang, J. Sun, C. Wang, *Science* **2024**, *386*, 693.
- [5] a) J. Huang, X. Han, S. Yang, Y. Cao, C. Yuan, Y. Liu, J. Wang, Y. Cui, *J. Am. Chem. Soc.* **2019**, *141*, 8996; b) B. Gui, X. Liu, Y. Cheng, Y. Zhang, P. Chen, M. He, J. Sun, C. Wang, *Angew. Chem., Int. Ed.* **2022**, *61*, e202113852.
- [6] a) Y. Zhang, Z. Qiao, R. Zhang, Z. Wang, H. J. Wang, J. Zhao, D. Cao, S. Wang, *Angew. Chem., Int. Ed.* **2023**, *62*, e202314539; b) P. Dong, X. Xu, R. Luo, S. Yuan, J. Zhou, J. Lei, *J. Am. Chem. Soc.* **2023**, *145*, 15473.
- [7] a) Y. Zhang, J. Duan, D. Ma, P. Li, S. Li, H. Li, J. Zhou, X. Ma, X. Feng, B. Wang, *Angew. Chem., Int. Ed.* **2017**, *56*, 16313; b) Y. Hu, N. Dunlap, S. Wan, S. Lu, S. Huang, I. Sellinger, M. Ortiz, Y. Jin, S. H. Lee, W. Zhang, *J. Am. Chem. Soc.* **2019**, *141*, 7518.
- [8] a) F. J. Uribe-Romo, J. R. Hunt, H. Furukawa, C. Klock, M. O'Keeffe, O. M. Yaghi, *J. Am. Chem. Soc.* **2009**, *131*, 4570; b) H. Li, J. Ding, X. Guan, F. Chen, C. Li, L. Zhu, M. Xue, D. Yuan, V. Valtchev, Y. Yan, S. Qiu, Q. Fang, *J. Am. Chem. Soc.* **2020**, *142*, 13334.
- [9] X. Ma, T. F. Scott, *Commun. Chem.* **2018**, *1*, 98.
- [10] Y. Jin, Y. Hu, M. Ortiz, S. Huang, Y. Ge, W. Zhang, *Chem. Soc. Rev.* **2020**, *49*, 4637.
- [11] E. Jin, K. Geng, K. H. Lee, W. Jiang, J. Li, Q. Jiang, S. Irle, D. Jiang, *Angew. Chem., Int. Ed.* **2020**, *59*, 12162.
- [12] a) B. P. Biswal, S. Chandra, S. Kandambeth, B. Lukose, T. Heine, R. Banerjee, *J. Am. Chem. Soc.* **2013**, *135*, 5328; b) N. L. Campbell, R. Clowes, L. K. Ritchie, A. I. Cooper, *Chem. Mater.* **2009**, *21*, 204.
- [13] a) P. F. Wei, M. Z. Qi, Z. P. Wang, S. Y. Ding, W. Yu, Q. Liu, L. K. Wang, H. Z. Wang, W. K. An, W. Wang, *J. Am. Chem. Soc.* **2018**, *140*, 4623; b) P. L. Wang, S. Y. Ding, Z. C. Zhang, Z. P. Wang, W. Wang, *J. Am. Chem. Soc.* **2019**, *141*, 18004.
- [14] a) C. Qian, Q. Y. Qi, G. F. Jiang, F. Z. Cui, Y. Tian, X. Zhao, *J. Am. Chem. Soc.* **2017**, *139*, 6736; b) P. J. Waller, Y. S. AlFaraj, C. S. Diercks, N. N. Jarenwattananon, O. M. Yaghi, *J. Am. Chem. Soc.* **2018**, *140*, 9099; c) M. C. Daugherty, E. Vitaku, R. L. Li, A. M. Evans, A. D. Chavez, W. R. Dichtel, *Chem. Commun.* **2019**, *55*, 2680.
- [15] W. Zhang, L. Chen, S. Dai, C. Zhao, C. Ma, L. Wei, M. Zhu, S. Y. Chong, H. Yang, L. Liu, Y. Bai, M. Yu, Y. Xu, X. W. Zhu, Q. Zhu, S. An, R. S. Sprick, M. A. Little, X. Wu, S. Jiang, Y. Wu, Y. B. Zhang, H. Tian, W. H. Zhu, A. I. Cooper, *Nature* **2022**, *604*, 72.
- [16] A. M. Evans, L. R. Parent, N. C. Flanders, R. P. Bisbey, E. Vitaku, M. S. Kirschner, R. D. Schaller, L. X. Chen, N. C. Gianneschi, W. R. Dichtel, *Science* **2018**, *361*, 52.
- [17] X. Guan, Y. Ma, H. Li, Y. Yusran, M. Xue, Q. Fang, Y. Yan, V. Valtchev, S. Qiu, *J. Am. Chem. Soc.* **2018**, *140*, 4494.
- [18] a) N. Huang, X. Ding, J. Kim, H. Ihee, D. Jiang, *Angew. Chem., Int. Ed.* **2015**, *54*, 8704; b) T. Jadhav, Y. Fang, C. H. Liu, A. Dadvand, E. Hamzehpoor, W. Patterson, A. Jonderian, R. S. Stein, D. F. Perepichka, *J. Am. Chem. Soc.* **2020**, *142*, 8862.
- [19] Z. Li, X. Ding, Y. Feng, W. Feng, B.-H. Han, *Macromolecules* **2019**, *52*, 1257.
- [20] O. M. Yaghi, M. J. Kalmutzki, C. S. Diercks, *Introduction to Reticular Chemistry: Metal-Organic Frameworks and Covalent Organic Frameworks*, Wiley-VCH, Weinheim, Germany, **2019**, pp.177–195.
- [21] T. Ma, J. Li, J. Niu, L. Zhang, A. S. Etman, C. Lin, D. Shi, P. Chen, L. H. Li, X. Du, J. Sun, W. Wang, *J. Am. Chem. Soc.* **2018**, *140*, 6763.
- [22] T. Ma, E. A. Kapustin, S. X. Yin, L. Liang, Z. Zhou, J. Niu, L. H. Li, Y. Wang, J. Su, J. Li, X. Wang, W. D. Wang, W. Wang, J. Sun, O. M. Yaghi, *Science* **2018**, *361*, 48.
- [23] S. Y. Ding, X. H. Cui, J. Feng, G. Lu, W. Wang, *Chem. Commun.* **2017**, *53*, 11956.
- [24] J. Yang, S. Ghosh, J. Roeser, A. Acharjya, C. Penschke, Y. Tsutsui, J. Rabeah, T. Wang, S. Y. Djoko Tameu, M. Y. Ye, J. Gruneberg, S. Li, C.

- Li, R. Schomacker, R. Van De Krol, S. Seki, P. Saalfrank, A. Thomas, *Nat. Commun.* **2022**, *13*, 6317.
- [25] H. L. Nguyen, C. Gropp, N. Hanikel, A. Mockel, A. Lund, O. M. Yaghi, *ACS Cent. Sci.* **2022**, *8*, 926.
- [26] P. Guan, J. Qiu, Y. Zhao, H. Wang, Z. Li, Y. Shi, J. Wang, *Chem. Commun.* **2019**, *55*, 12459.
- [27] R. E. Maleczka, F. Shi, D. Holmes, M. R. Smith, *J. Am. Chem. Soc.* **2003**, *125*, 7792.
- [28] a) J. Xu, X. Wang, C. Shao, D. Su, G. Cheng, Y. Hu, *Org. Lett.* **2010**, *12*, 1964; b) E. Kianmehr, M. Yahyaee, K. Tabatabai, *Tetrahedron Lett.* **2007**, *48*, 2713; c) S. P. Pitre, C. D. McTiernan, H. Ismaili, J. C. Scaiano, *J. Am. Chem. Soc.* **2013**, *135*, 13286; d) Y. Q. Zou, J. R. Chen, X. P. Liu, L. Q. Lu, R. L. Davis, K. A. Jorgensen, W. J. Xiao, *Angew. Chem., Int. Ed.* **2012**, *51*, 784; e) K. Hosoi, Y. Kuriyama, S. Inagi, T. Fuchigami, *Chem. Commun.* **2010**, *46*, 1284.
- [29] a) M. Kim, J. F. Cahill, H. Fei, K. A. Prather, S. M. Cohen, *J. Am. Chem. Soc.* **2012**, *134*, 18082; b) P. Deria, J. E. Mondloch, O. Karagiari, W. Bury, J. T. Hupp, O. K. Farha, *Chem. Soc. Rev.* **2014**, *43*, 5896; c) S. Pullen, G. H. Clever, *Acc. Chem. Res.* **2018**, *51*, 3052.